JOURNAL OF THERMOPHYSICS AND HEAT TRANSFER
Vol. 6, No. 4, Oct.–Dec. 1992

Combined Natural Convection and Radiation from Heated Cylinders Inside a Container

Z. Zhao,* D. Poulikakos,† and Z. Ren‡
University of Illinois at Chicago, Chicago, Illinois 60680

In this article a numerical investigation verified by experiments is reported on steady-state heat transfer from three electrically heated cylinders equally spaced and resting at the bottom wall of a rectangular container. The investigation simulates heat transfer from power cables sparsely laid inside rectangular trays. The results indicate that a multicellular flow pattern existed in the system. At high Grashof numbers, the flow in the right half of the system consisted of a large cell rotating above the cylinders and two small cells trapped between the cylinders. Results for the average Nusselt number and the average and maximum temperature of the center cylinder are also reported in the present study. The average Nusselt number differs markedly from that for a single cylinder in an infinite space underlining the importance of the interaction of the cylinders with each other and with the container. The spacing of the cylinders had a visible effect on the magnitude and the location of the maximum temperature of the center cylinder.

Nomenclature

A_i = surface area
b = thickness of enclosure wall, m, Fig. 1
D = cylinder diameter, m, Fig. 1
F_{ij} = configuration factor
Gr = Grashof number, Eq. (8)
g = gravitational acceleration, m/s^2
H = height of the enclosure, m
h = local convective heat transfer coefficient, w/m^2·K
$\bar{h}$ = average convective heat transfer coefficient, w/m^2·K
h_j = average natural convection heat transfer coefficient between the jth outer surface and the ambient, w/m^2·K, Eq. (26)
J_i = dimensionless radiosity of the ith surface, Eq. (12)
$\hat{J}_i$ = radiosity of the ith surface, w/m^2
k = thermal conductivity of air, w/m·K
k_c = thermal conductivity of the enclosure wall, w/m·K
L = length of the cylinder
M = number of grid lines in x-direction
N = number of grid lines in y-direction
$\underline{Nu}$ = local Nusselt number, Eq. (34)
$\overline{Nu}$ = average Nusselt number, Eq. (25)
n = distance normal to the wall, m
Pr = Prandtl number, Eq. (7)
$\dot{q}'$ = heat generation per unit length of cylinder, w/m
$\dot{q}'_{r1}$ = dimensionless net radiative heat transfer rate per unit length from the central cylinder
$\dot{q}'_{r2}$ = dimensionless net radiative heat transfer rate per unit length from the right cylinder
$\dot{q}'_{r3}$ = dimenionless net radiative heat transfer rate per unit length from the enclosure
R_j = dimensionless thermal resistance, Eq. (26)
s = cylinder spacing, Fig. 1
T = temperature, K
T_∞ = ambient temperature, K
t = dimensionless time, Eq. (6)
u = dimensionless velocity in x direction, Eq. (6)
v = dimensionless velocity in y direction, Eq. (16)
W = width of the enclosure, m
x = dimensionless horizontal coordinate, Eq. (6)
y = dimensionless vertical coordinate, Eq. (6)
α = thermal diffusivity, m^2/s
β = volumetric thermal expansion coefficient, K^{-1}
γ = position angle, Fig. 1
ε_i = emissivity of the ith surface
θ = dimensionless temperature, Eq. (6)
θ_i = dimensionless average temperature of the ith surface
θ_∞ = dimensionless ambient temperature
ν = kinematic viscosity, m^2/s
ξ_1, ξ_2, ξ_3 = positive coefficients, Eqs. (30) and (31)
σ = Stefan-Boltzmann constant
ψ = dimensionless streamfunction, Eq. (6)
ω = dimensionless vorticity, Eq. (6)

Subscript
$\hat{}$ = denotes dimensional quantity

Superscript
∞ = denotes room conditions

I. Introduction

IN this article, the results of a study of combined natural convection and radiation from three parallel horizontal cylinders enclosed in a container are reported. The cylinders model power cables sparsely laid at the bottom surface of an enclose rectangular tray. Relevant to the present work are studies of heat transfer between "inner" bodies and their surrounding enclosure. In the following paragraphs, representatives of such studies are reviewed.

Warrington and Crupper[1] investigated the phenomenon of natural convection heat transfer between a bundle of tubes and a cubical enclosure surrounding the tubes. They showed that cell formation between the inner bodies (tubes) intensified the natural convection in the enclosure. Babus'Haq et al.[2,3] studied pipeline arrangements in underground tunnels

Received Aug. 5, 1991; revision received Sept. 27, 1991; accepted for publication Sept. 30, 1991.
*Graduate Student.
†Associate Professor.
‡Professor, Thermal Engineering Department, Tsinghua University, Beijing 100084, People's Republic of China.

in district heating applications. They reported that the heat losses were affected by the relative position of the high- and low-temperature tubes in the tunnel. Sparrow and co-workers have carried out several studies on the heat transfer between an enclosure and the inner bodies that it surrounds. For example, Sparrow et al.[4] investigated the phenomenon of natural convection in enclosures with off-center inner bodies. Sparrow and Charmchi[5] carried out experiments on natural convection in an enclosure formed between eccentric and concentric vertical cylinders of different height and diameter.

The present work is a numerical study, complemented with experimental verification of the problem of cooling of three horizontal cylinders placed at the bottom wall of a rectangular enclosure. The cooling is achieved by the combined action of natural convection and radiation. The results of the study document the effect of interaction of the cylinders with each other and with the container on the temperture and flowfields and on the convective heat transport. Radiation is found to be important. Overall, the present study reveals interesting trends, from the heat transfer standpoint, that should be taken into account when the proper placement of power cables in trays is decided.

II. Mathematical Formulation

The system of interest is shown in Fig. 1. The enclosed container is of length W and height H. The three cylinders are equally spaced. The spacing is denoted by s. The various surfaces are numbered from one to four to facilitate the radiation modeling that is discussed later in this section. The cylinders are heated electrically and they dissipate $\dot{q}'$ (W/m) at their surface. The container is assumed to communicate thermally with the environment; that is, natural convection is assumed to take place between the outer surfaces of the walls of the container and the environment. The mathematical model for the combined natural convection-radiation cooling of the heated cylinders in the setting described above is discussed next.

A. Natural Convection Inside the Container

The dimensionless, Boussinesq—approximated, governing equations describing the process of buoyancy-driven convection in the container are

$$\frac{\partial^2\psi}{\partial x^2} + \frac{\partial^2\psi}{\partial y^2} = -\omega \tag{1}$$

$$\frac{\partial\omega}{\partial t} + u\frac{\partial\omega}{\partial x} + v\frac{\partial\omega}{\partial y} = Gr\frac{\partial\theta}{\partial x} + \frac{\partial^2\omega}{\partial x^2} + \frac{\partial^2\omega}{\partial y^2} \tag{2}$$

$$\frac{\partial\theta}{\partial t} + u\frac{\partial\theta}{\partial x} + v\frac{\partial\theta}{\partial y} = \frac{1}{Pr}\left[\frac{\partial^2\theta}{\partial x^2} + \frac{\partial^2\theta}{\partial y^2}\right] \tag{3}$$

Equation (1) is the definition of vorticity ω. Equation (2) is the vorticity conservation equation obtained by cross-differentiating and subtracting the two momentum equations (in the x and in the y directions). As byproduct of this process, the pressure gradient terms in the momentum equations are eliminated. Equation (3) is the energy equation. The streamfunction ψ was defined in the usual manner

$$u = \frac{\partial\psi}{\partial y} \tag{4}$$

$$v = -\frac{\partial\psi}{\partial x} \tag{5}$$

The usual Boussinesq approximation adopted in Eqs. (1–3) states that the density of the fluid is constant everywhere except in the body force term of the momentum equation, where it is assumed to vary linearly with the temperature.

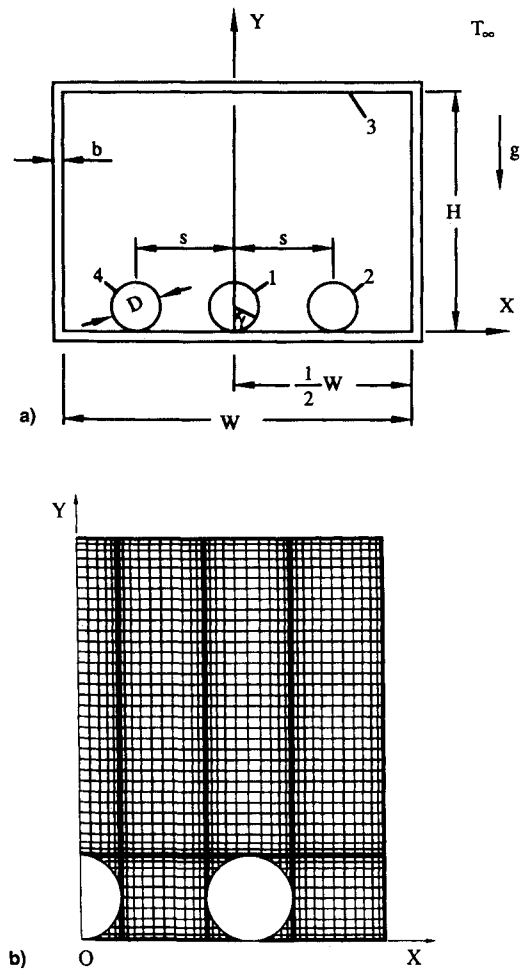

Fig. 1 a) Schematic of the system of interest, and b) the grid utilized for the numerical solution.

The nondimensionalization process was carried out based on the following definitions

$$x = \frac{\hat{x}}{D},\quad y = \frac{\hat{y}}{D},\quad u = \frac{\hat{u}}{\nu/D},\quad v = \frac{\hat{v}}{\nu/D},\quad \theta = \frac{T}{\dot{q}'/\pi k},$$

$$\psi = \frac{\hat{\psi}}{\nu/D^2},\quad \omega = \frac{\hat{\omega}}{\nu/D^2},\quad t = \frac{\hat{t}}{D^2/\nu} \tag{6}$$

The nondimensionalization process yielded the appearance of the Prandtl and the Grashof numbers defined as follows:

$$Pr = \nu/\alpha \tag{7}$$

$$Gr = \frac{g\beta(\dot{q}'/\pi k)D^3}{\nu^2} \tag{8}$$

B. Radiation Heat Transfer Inside the Container

To model the radiation heat transfer in the cavity, we considered the radiative heat exchange arrangement shown in Fig. 1. The dimensionless energy balances for surfaces 1, 2, and 3 (realizing that surface 2 is identical to surface 4; i.e., the radiative heat exchange for the left cylinder is identical to that for the right cylinder) are as follows[6]:

$$-\frac{1}{1-\varepsilon_1}J_1 + (F_{12} + F_{14})J_2 + F_{13}J_3 = \frac{\varepsilon_1\theta_1^4}{\varepsilon_1 - 1} \tag{9}$$

$$F_{21}J_1 + \left(-\frac{1}{1-\varepsilon_2}\right)J_2 + F_{23}J_3 = \frac{\varepsilon_2\theta_2^4}{\varepsilon_2 - 1} \tag{10}$$

$$F_{31}J_1 + (F_{32} + F_{34})J_2 + \left(F_{33} - \frac{1}{1 - \varepsilon_3}\right) J_3 = \frac{\varepsilon_3\theta_3^4}{\varepsilon_3 - 1} \quad (11)$$

In the above equations J_i ($i = 1, 2, 3$) is the dimensionless radiosity

$$J_i = \frac{\hat{J}_i}{\sigma(\dot{q}'/\pi k)^4} \quad (12)$$

Note that if the dimensionless radiosity is known, the net dimensionless radiation heat transfer rate can be calculated from the following equations[6]:

$$\dot{q}'_{ri} = \frac{\hat{\dot{q}}'_{ri}}{\sigma A_i(\dot{q}'/\pi k)^4} = \frac{\theta_i^4 - J_i}{(1 - \varepsilon_i)/\varepsilon_i} \qquad i = 1, \ldots, 3 \quad (13)$$

The configuration factors in Eqs. (9–11) are obtained from Siegel and Howell[6]

$$F_{12} = F_{14} = \frac{1}{\pi}\left[\sqrt{\left(\frac{s}{D}\right)^2 - 1} + \tan^{-1}\frac{1}{\sqrt{\left(\frac{s}{D}\right)^2 - 1}} - \frac{s}{D}\right] \quad (14)$$

$$F_{13} = 1 - 2F_{12} \quad (15)$$

$$F_{21} = F_{12} \quad (16)$$

$$F_{23} = 1 - F_{12} \quad (17)$$

$$F_{24} = 0 \quad (18)$$

$$F_{31} = \frac{A_1}{A_3} F_{13} \quad (19)$$

$$F_{32} = \frac{A_2}{A_3} F_{23} \quad (20)$$

$$F_{33} = 1 - \frac{A_1}{A_3}(3 - 4F_{12}) \quad (21)$$

C. Boundary and Initial Conditions at the Various Surfaces

The boundary conditions for the temperature and the velocity fields at the various surfaces are as follows:

On the Surface of the Cylinders

$$u = v = \psi = 0 \quad (22)$$

$$1 = -\left(\frac{\partial\theta}{\partial n}\right)_{\text{cylinder surface}} + \frac{D\sigma(\dot{q}'/\pi k)^3}{k}\dot{q}'_{ri} \quad (23)$$

where n is the dimensionless normal direction to the cylinder surface ($n = \hat{n}/D$). Equation (22) stands for the no-slip and the no-penetration conditions at the cylinder surface, while Eq. (23) states the fact that the heat generated electrically at the cylinder is removed by the combined action of natural convection and radiation. Note that Eq. (23) needs to be applied only to cylinders 1 and 2 because the behavior of cylinder 4 is identical to that of cylinder 1. As a matter of fact, the flow and temperature fields in the system of Fig. 1 are symmetric about the vertical plate passing through the center of the middle cylinder. As discussed later, this symmetry will be utilized in the numerical solution to save computational time.

On the Walls of the Container

$$u = v = \psi = 0 \quad (24)$$

$$-\left(\frac{\partial\theta}{\partial n}\right)_j - \frac{D\sigma(\dot{q}'/\pi k)^3}{k}\dot{q}'_{rj} = \frac{\theta_j - \theta_\infty}{R_j}, \quad j = T, S, B \quad (25)$$

The values T, S, B that the index j assumes stand for the top the side and the bottom wall of the container, respectively. The left-hand side of Eq. (25) accounts for the convection and radiation at the inner surface of the container. The right-hand side of Eq. (25) accounts for the natural convection cooling of the outer surface of the container by the "room" air of temperature T_∞. The dimensionless thermal resistance R_j caused by the combined action of the wall material and the natural convection thermal boundary layer at the outer surface of the container wall is

$$R_j = k/Dh_j + kb/Dk_c, \quad j = T, S, B \quad (26)$$

where b is the thickness of the container wall, k_c the conductivity of the container wall, and h_j is the heat transfer coefficient between the top, side, or bottom container walls and the ambient. Values for h_j for flat plate natural convection available in the literature[7] were utilized in this study.

On the Plane of Symmetry

$$u = \psi = \omega = \frac{\partial\theta}{\partial x} = 0 \quad (27)$$

Initial Conditions

The system was assumed to be initially isothermal (at room temperature) and motionless

$$t = 0: u = v = \psi = \omega = 0 \quad \text{everywhere} \quad (28)$$

$$t = 0: \quad \theta = \theta_\infty \quad \text{everywhere} \quad (29)$$

III. Numerical Solution

The mathematical model described earlier was solved earlier with the method of false transient.[8–10] To this end, the governing Eqs. (1–3) were cast in the following (1–3) "false" form:

$$\frac{\partial\psi}{\partial t} - \xi_1\left(\frac{\partial^2\psi}{\partial x^2} + \frac{^2\psi}{\partial y^2} + \omega\right) = 0 \quad (30)$$

$$\xi_2\frac{\partial\omega}{\partial t} + u\frac{\partial\omega}{\partial x} + v\frac{\partial\omega}{\partial y} = Gr\frac{\partial\theta}{\partial x} + \frac{\partial^2\omega}{\partial x^2} + \frac{\partial^2\omega}{\partial y^2} \quad (31)$$

$$\xi_3\frac{\partial\theta}{\partial t} + u\frac{\partial\theta}{\partial x} + v\frac{\partial\theta}{\partial y} = \frac{1}{Pr}\left(\frac{\partial^2\theta}{\partial x^2} + \frac{\partial^2\theta}{\partial y^2}\right) \quad (32)$$

where ξ_1, ξ_2, ξ_3 are positive coefficients. These coefficients allow for different time "response" of each equation to a specific time-step and facilitate convergence. In the steady-state (which is the only concern of the present study) the transient terms in Eqs. (30–31) become identically zero and the resulting temperature and flowfields satisfy the "true" conservation Eqs. (1–3). This method is well established in the literature[8–10] and no further details need to be given here.

After finite differencing, Eqs. (30–32) were solved in the right half of the physical domain shown in Fig. 1 by using the ADI method. At each time-step, utilizing the new values of θ_1, θ_2, θ_3 the system of Eqs. (9–11) was solved for J_1, J_2, J_3.

Subsequently $\dot{q}'_{r1}$, $\dot{q}'_{r2}$, $\dot{q}'_{r3}$ were obtained from Eq. (13) and were used to update boundary conditions (23, 25). The process was repeated at each time-step until convergence was achieved. The steady-state was defined by the following criterion:

$$\left| \frac{f_{i,j}^{\text{old}} - f_{i,j}^{\text{new}}}{f_{i,j}^{\text{new}}} \right| \leq 10^{-6} \quad i = 1, \ldots, m; \quad j = 1, \ldots, n \tag{33}$$

where f is ψ, ω, or θ, m is the number of vertical gridlines, and n is the number of horizontal gridlines. To this end, a nonuniform, rectangular grid was utilized. The terms "old" and "new" denote two sequential time-steps. The grid was denser in the neighborhood of the cylinders and the vertical walls of the container. A sample of the grid utilized is shown in Fig. 1b. Notice that the surface of each cylinder coincides with the lowermost grid point of each grid line intersecting the cylinder. Most runs of this study were performed on a grid $m \times n = 43 \times 46$ applied to the right "half" of the configuration in Fig. 1. Increasing the number of grid points did not change the results appreciably. For example, adding 10 grid lines in each direction changed the convective heat transfer rate from the center cylinder by less than one percent. Most of the additional grid lines were placed near the cylinder and near the container wall.

The results for the convective heat transfer rate from the cylinders will be presented with the help of the local and the average Nusselt numbers defined as

$$Nu = \frac{hD}{k} = -\frac{1}{\theta_w - \theta_\infty}\left(\frac{\partial\theta}{\partial n}\right)_w \tag{34}$$

$$\overline{Nu} = \frac{\bar{h}D}{k} = -\frac{1}{2\pi}\int_0^{2\pi} \frac{(\partial\theta/\partial n)_w}{\theta_w - \theta_\infty}\, d\gamma \tag{35}$$

where h, and $\bar{h}$ are the local and the average heat transfer coefficients, respectively, subscript w denotes the cylinder wall, subscript ∞ denotes the reference (room) temperature, and γ denotes the position angle around the cylinder. The remaining symbols were defined earlier. It is worth clarifying that the normal to the wall derivative of the temperature utilized in Eqs. (34, 35) was evaluated from the following equation:

$$\left(\frac{\partial\theta}{\partial n}\right)_w = \sqrt{\left(\frac{\partial\theta}{\partial x}\right)_w^2 + \left(\frac{\partial\theta}{\partial y}\right)_w^2} \tag{36}$$

The temperature derivatives with respect to x and y at the wall were discretized with the help of three point finite differences.[10]

It is obvious from the numerical model that the values of several parameters need to be specified at the outset of the numerical simulations. To this end, the emissivities were[6] $\varepsilon_1 = \varepsilon_2 = 0.94$ and $\varepsilon_3 = 0.84$. The container was assumed to be $b = 5$-mm thick and made out of plexiglas ($k_c = 0.195$ W/mK). The values of the heat transfer coefficient at the three surfaces of the container were taken from the literature[7] for laminar natural convection from a horizontal upward-facing plate, a vertical plate, and a horizontal downward-facing plate. Finally, the total heat transfer rate per unit length at the cable needed in boundary condition (23) was obtained from the definition of the Grashof number, Eq. (8), after a value for Gr was assigned.

IV. Experimental Verification Procedure

To provide verification of the numerical results a small-scale experiment was performed that aimed at flow visualization in the container, as well as at obtaining measurements of the average temperature of the cylinders. Three brass cylinders of diameter $D = 50$ mm and length $L = 690$ mm were placed parallel to each other at the bottom of a rectangular enclosure. The enclosure was made out of plexiglas of thickness $b = 5$ mm. Its height was $H = 236$ mm, its width $W = 356$ mm and its length $L = 700$ mm, only slightly longer than the brass cylinder. Three identical cartridge heaters were installed inside the brass tubes. Direct current was supplied to the heaters with the help of three power supplies. The power input to the heaters was measured with 3 Wm accurate within

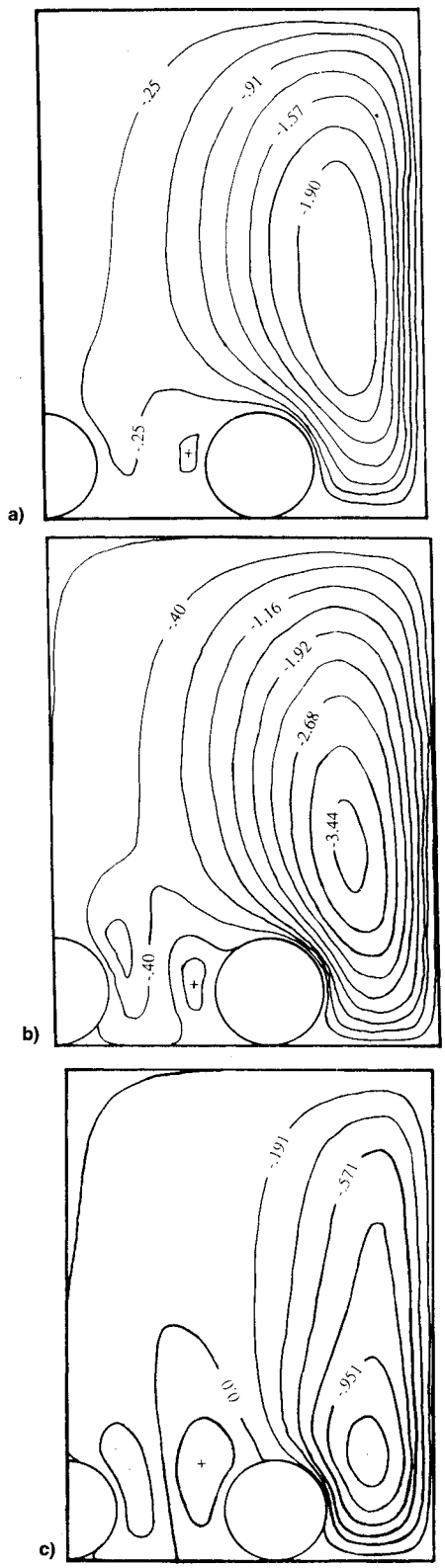

Fig. 2 Streamline patterns for $s = 100$ mm: a) $Gr = 2 \times 10^6$; b) $Gr = 4 \times 10^6$; and c) $Gr = 6.5 \times 10^6$.

0.5%. The power input to the three cylinders was identical. The temperature of the surface of each cylinder was measured with the help of thermocouples. Six thermocouples-per-cylinder were used spaced at 60 deg increments around the periphery. The average temperature of the center cylinder reported in this study was simply the arithmetic mean of the temperatures recorded by these six thermocouples. Steady state was obtained about 4 h after the power to the heaters was turned on. All measurements and observations reported in this study were obtained at steady-state conditions.

The flow in the system was visualized utilizing a light sheet technique. The light sheet was 5 mm thick and was produced by a 1000-W iodine-tungsten lamp installed in a black box with a narrow slot at its bottom. The sheet was placed such that it coincided with a plane perpendicular to the axis of the cylinders near the center of the enclosure. To trace the flow both zinc stearate ($Zn[C_{12}H_{35}O_2]_2$) particles and cigarette smoke were tried. Of these two tracers, smoke presented several problems. For example, it could not easily reach the region between the cylinders, it drifted randomly and it diffused rather fast. Because of these drawbacks smoke was abandoned. The zinc stearate particles, on the other hand, performed much better and were used in all the flow visualization photographs reported later in this study. These particles are water-insoluble and have good light-scattering properties. Aihara et al.[11] have used these particles to calculate the velocity field in an experiment with air as the working fluid.

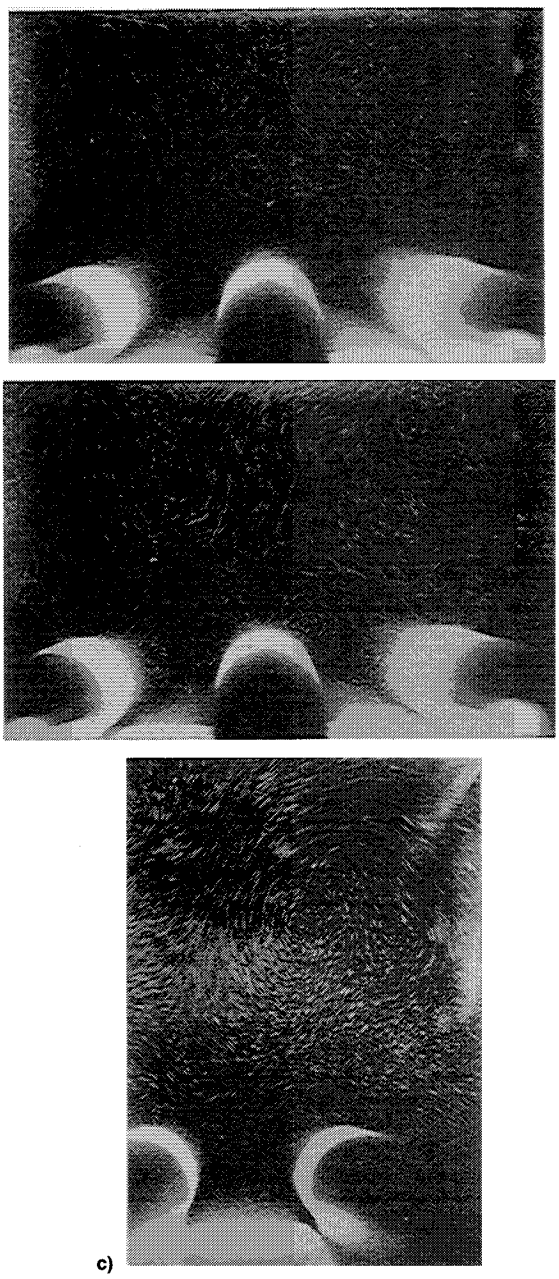

Fig. 3 Flow visualization for s = 100 m: a) $Gr = 2 \times 10^6$; b) $Gr = 4 \times 10^6$; and c) $Gr = 6.5 \times 10^6$.

In the present study, photographs of the flowfield were taken at least 30 minutes after the introduction of the zinc stearate particles in the enclosure. A 35-mm camera was used with a 400 ASA film and an exposure time of $\frac{1}{8}$ s at F 1.4.

V. Results and Discussion

The presentation of the results begins with typical flow and temperature fields in the container. Figure 2 shows sets of streamlines for three representative Grashof numbers. For $Gr = 2 \times 10^6$ (Fig. 2a), the flow in the right half of the enclosure consists mainly of a single cell circulating clockwise. It rises above the center cylinder as well as above the right cylinder and descends along the colder right vertical wall of the enclosure. The center of rotation of this cell is close to the side wall of the container. The downflow near this wall is faster than the upflow above the cylinders.

Interestingly, a small counterclockwise rotating vortex (cell) was observed forming in the region between the center and the right cylinder, closer to the right cylinder. Part of the fluid in the main cell discussed earlier flows on top of the counterclockwise vortex between the cylinders. Increasing the Grashof number further to $Gr = 4 \times 10^6$ (Fig. 2b) and eventually to $Gr = 6.5 \times 10^6$ (Fig. 2c) initiated the existence of a third cell in the region between the center and the right cylinder. This third cell rotates clockwise and is of similar size to the second cell, together with which it occupies the region between the two cylinders. The existence of the third cell is speculated to be a result of the interaction between the upward moving fluid emanating from the center cylinder and the small counterclockwise rotating vortex occupying the region between the two cylinders. Increasing the Grashof number from $Gr = 4 \times 10^6$ to $Gr = 6.5 \times 10^6$ moved the above-mentioned third cell lower between the two cylinders and also shifted the center of rotation of the large cell downwards.

Figure 3 shows the results on the steady-state flowfield obtained by the flow visualization. The Grashof numbers in Figs. 3a, 3b, and 3c are practically identical to those of Figs. 2a, 2b, and 2c, respectively. The similarity between the experimental findings of Fig. 3 and the numerical predictions of Fig. 2 is obvious. First, the flowfield is indeed symmetric about the midplane of the system. Second, the flow in the right half of the system above the cylinders consists of a single large cell. Third, a small cell does develop between the two adjacent cylinders for $Gr = 2 \times 10^6$ (Fig. 3a) closer to the side cylinder. Finally, increasing the Grashof number to $Gr = 4 \times 10^6$ and to $Gr = 6.5 \times 10^6$ (Figs. 3b and 3c, respectively) gives rise to a third cell between the two cylinders. The findings of Fig. 3 add credibility and verify the numerical predictions of Fig. 2.

Figure 4 shows maps of isotherms in the right half of the system for the same Grashof numbers corresponding to the streamlines of Fig. 2. Clearly, going from Fig. 4a to Fig. 4c shows that increasing the Grashof number (the heat output of the cylinders) yields higher temperature throughout the system. The downward bending in the 34°C isotherm of Fig. 4b and in the 42°C isotherm of Fig. 4c is caused by the two smaller cells rotating between the two cylinders. The dense spacing of the isotherms in the vicinity of the cylinders indicates that the temperature gradients and, therefore, the heat transfer rates in this vicinity are the highest observed in the system.

Because it is expected that the cooling of the central cylinder will be the "worst" compared to the other cylinders and, therefore, that this cylinder is most likely to present overheating problems, the discussion of additional results is focused on the central cylinder. The effect of Gr on the av-

erage temperature of the central cylinder is shown in Fig. 5. The numerical and the experimental findings show good agreement and illustrate that the average temperature of the center cylinder increases significantly and almost linearly with increasing *Gr*. Note that the temperature variation around the periphery of the cylinders was rather small, less than 2°C.

Of interest is the dependence of the maximum temperature of the center cylinder on the cylinder spacing *s*. In the power cable application, exceedingly high temperatures caused by placing the cables too close to each other may cause cable burnout and disrupt the cable operation. Figures 6a and 6b show the position and the magnitude of the maximum temperature of the middle cylinder, respectively. Clearly, as the spacing between cylinders decreases, the location of the maximum temperature on the right half of the central cylinder is attracted toward the right cylinder (Fig. 6a). As the spacing

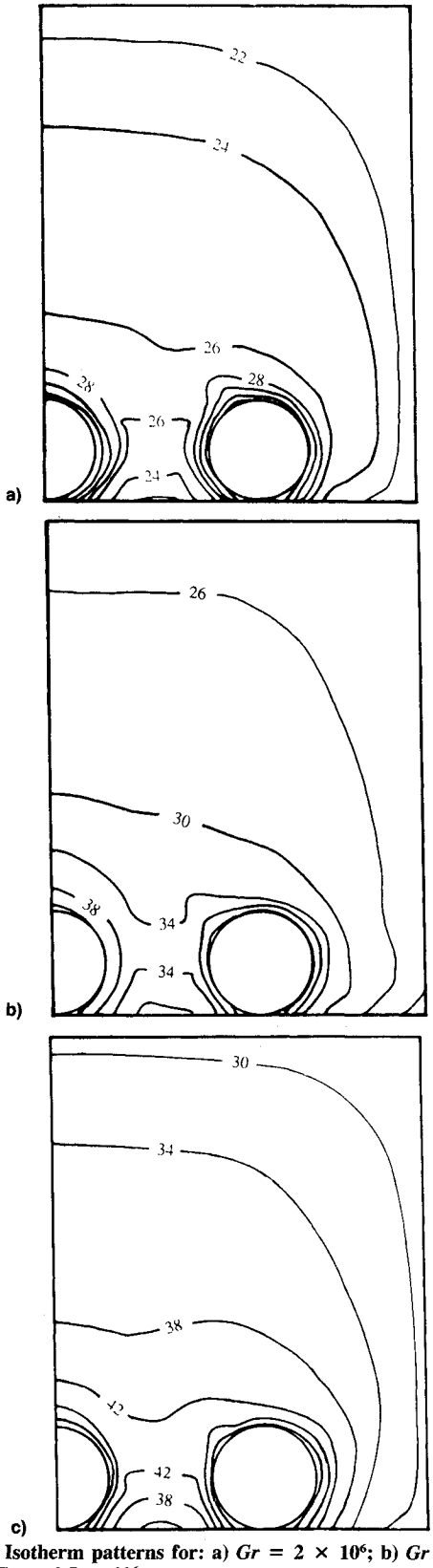

Fig. 4 Isotherm patterns for: a) $Gr = 2 \times 10^6$; b) $Gr = 4 \times 10^6$; and c) $Gr = 6.5 \times 10^6$.

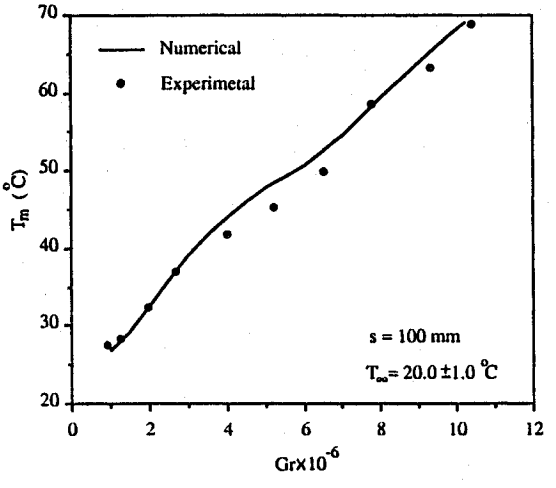

Fig. 5 The dependence of the average temperature of the central cylinder on *Gr* for *s* = 100 mm.

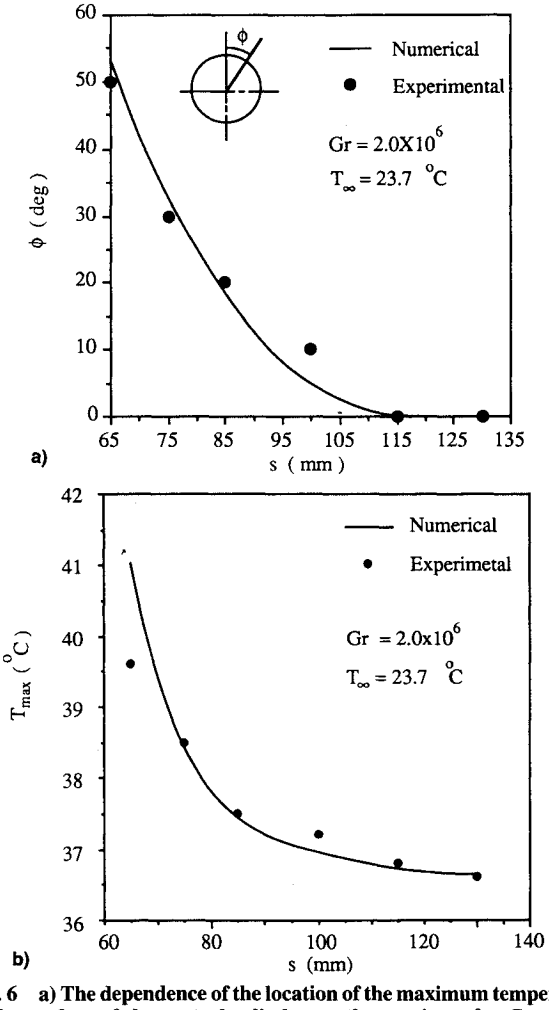

Fig. 6 a) The dependence of the location of the maximum temperature of the surface of the central cylinder on the spacing *s* for $Gr = 2 \times 10^6$, and b) the dependence of the magnitude of the maximum surface temperature of the central cylinder on the spacing *s* for $Gr = 2 \times 10^6$.

increases, the location of the maximum temperature shifts toward the vertical plane of symmetry. For $s \approx 115$ mm, the maximum temperature of the cylinder takes place at the place of symmetry ($\phi = 0$). Increasing the spacing further has no effect on the location of the maximum temperature. A decrease in the maximum temperature of about 4.5°C is observed if the spacing of the cylinders is increased from $s = 65$ mm to $s = 130$ mm (Fig. 6b). The general trend shown in Fig. 6b is that as the spacing increases, the maximum temperature of the central cylinder decreases until a plateau is reached after which the effect of s on the maximum temperature is minimal. The rate of decrease of the maximum temperature is steeper at smaller values of s.

The effect of radiation on the temperature field of the system of interest is illustrated in Fig. 7 for $Gr = 2 \times 10^6$. In this figure, horizontal temperature profiles throughout the x–y plane of Fig. 1 are shown both in the presence (Fig. 7a) and in the absence (Fig. 7b) of radiation. The presence of radiation yields better cooling and lower temperatures all around. In addition, the presence of radiation yields larger temperature variations between and closely above the cylinders. Overall, Fig. 7 indicates that radiation heat transfer is important in the problem under consideration and needs to be included in the modeling. Its omission could yield significant errors in predicting the temperature field (and, therefore, also the flowfield).

Figure 8 presents a comparison between the present results for the local Nusselt number of the central cylinder for $s = 100$ mm and $Gr = 1.4 \times 10^6$ and the results of Qureshi and

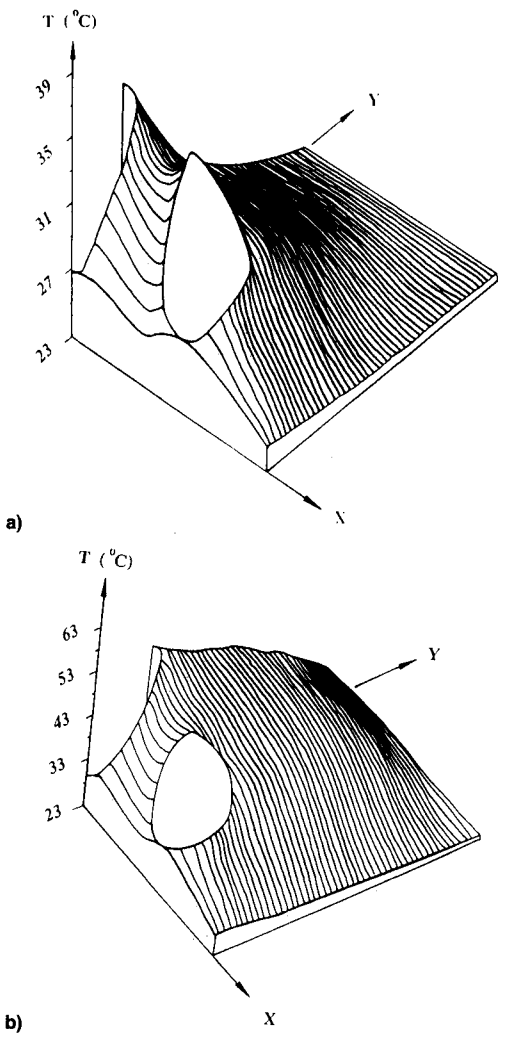

Fig. 7 Horizontal temperature profiles in the system for $s = 100$ mm and $Gr = 2 \times 10^6$; a) accounting for radiation, and b) not accounting for radiation.

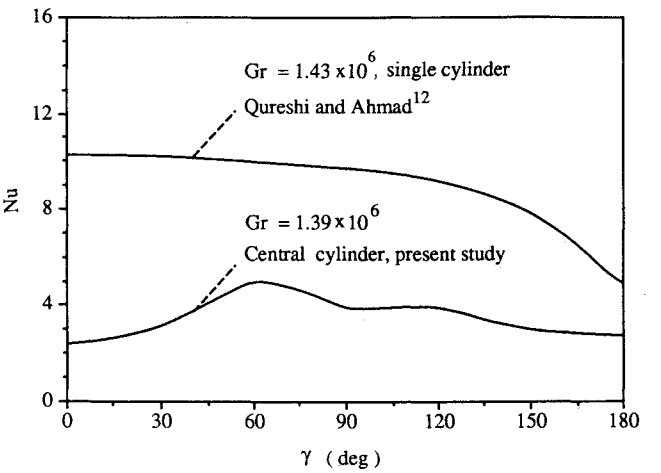

Fig. 8 Comparison of the local Nusselt number of the center cylinder of the present study to the local Nusselt number of Qureshi and Ahmad[12] for a single cylinder.

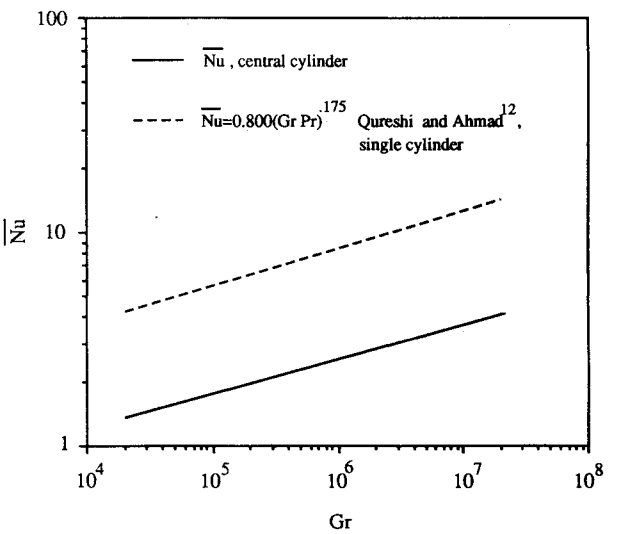

Fig. 9 The dependence of the average Nusselt number of the central cylinder on Gr.

Ahmad[12] for natural convection from a horizontal constant heat flux cylinder in an infinite air space. The purpose of this figure is to exemplify the effect of cylinder-to-cylinder and cylinder-to-container interaction on the local Nusselt number distribution. Clearly, the present values of Nu are considerably lower and exhibit different angular behavior. Unlike in the work of Qureshi and Ahmad,[12] where the maximum of the Nusselt number occurred at $\phi = 0°$, in our study the location of the maximum Nu is shifted toward the right cylinder ($\phi = 60°$).

Finally, the dependence of the average Nusselt number of the central cylinder on Gr is shown in Fig. 9. Clearly $\overline{Nu}$ increases monotonically with Gr. The dashed line represents the results of the numerical investigation by Qureshi and Ahmad[12] for natural convection from a single cylinder in an infinite space. The presence of the container and the neighboring cylinders drastically (almost by fourfold) decreases the overall convective heat transfer from the central cylinder. This result indicates that correlations for single cylinders should not be used to estimate the cooling of power cables in trays. Incorrect estimation of the cooling of these cables by neglecting the interaction with other cables and the container may cause serious overheating and damage.

VI. Conclusions

In this paper, a theoretical study including experimental verification was reported on the problem of heat transfer from

three electrically heated cylinders, resting at the bottom of a rectangular enclosure. The experiment aimed at simulating heat transfer from power cables placed inside trays. In the right half of the system, the flowfield above the cylinders consisted of a large clockwise rotating cell. As Gr increased, a single small cell appeared between the cylinders. A further increase of the value of Gr yielded a second cell in the region between the cylinders. It was shown that radiation heat transfer is important and needs to be included in the theoretical modeling of the problem. The maximum temperature of the central cylinder increased drastically as the cylinder spacing decreased. In addition, the location of this maximum on the cylinder surface was shifted away from the top of the cylinder, where it occurs when a single cylinder is cooled by natural convection in an infinite space. Finally, results for the local and the average Nusselt numbers showed significant deviations from results reported for single cylinders. Consequently, it is concluded that in placing power cables in trays existing correlations for single cylinders should not be used to estimate the cooling and the operating temperatures of these cables.

References

[1]Warrington, R. O., and Crupper, G., "Natural Convection Heat Transfer Between Cylindrical Tube Bundles and a Cubical Enclosure," *Journal of Heat Transfer,* Vol. 103, No. 1, 1981, pp. 103–107.

[2]Babus'Haq, R. F., Probert, S. D., Shilston, M. J., and Talati, A., "Suggested Design Improvements Concerning District Heating Pipeline Configurations," *Applied Energy*, Vol. 17, No. 2, 1984, pp. 77–96.

[3]Babus'Haq, R. F., Probert, S. D., and Shilston, M. J., "Natural Convection Across Cavities: Design Advice," *Applied Energy*, Vol. 20, No. 3, 1985, pp. 161–188.

[4]Sparrow, E. M., Stryker, P. C., and Ansri, M. A., "Natural Convection in Enclosures with Off-Centre Innerbodies," *International Journal of Heat and Mass Transfer,* Vol. 27, No. 1, 1984, pp. 49–56.

[5]Sparrow, E. M., and Charmchi, M., "Natural Convection Experiments in an Enclosure Between Eccentric and Concentric Vertical Cylinders of Different Height and Diameter," *International Journal of Heat and Mass Transfer,* Vol. 26, No. 1, 1983, pp. 133–143.

[6]Siegel, R., and Howell, J. R., *Thermal Radiation Heat Transfer,* 2nd ed., McGraw-Hill, NY, 1981.

[7]Incropera, F. P., and DeWitt, D. P., *Fundamentals of Heat Transfer,* Wiley, 1981, pp. 442–445.

[8]Mallinson, G. D., and DeVahl Davis, G., "The Method of False Transient for the Solution of Coupled Elliptic Equations," *Journal of Computational Physics*, Vol. 12, No. 4, 1973, pp. 435–461.

[9]DeVahl Davis, G., "Finite Difference Method for Natural and Mixed Convection in Enclosures," *Proceedings of the Eighth International Heat Transfer Conference,* Vol. 1, 1986, pp. 101–109.

[10]Roache, P. J., *Computational Fluid Dynamics,* Hermosa Pubs., Albuquerque, NM, 1976.

[11]Aihara, T., Yamada, Y., and Endo, S., "Free Convection Along the Downward-Facing Surface of a Heated Horizontal Plate," *International Journal of Heat and Mass Transfer,* Vol. 15, No. 12, 1972, pp. 2535–2549.

[12]Qureshi, Z. H., and Ahmad, R., "Natural Convection from a Uniform Heat Flux Horizontal Cylinder at Moderate Rayleigh Numbers," *Numerical Heat Transfer,* Vol. 11, No. 2, 1987, pp. 199–212.